

# Evaluation of Defect-Related Diffusion in Semiconductors by Electrooptical Sampling

Paul D. Biernacki, Henry Lee, and Alan R. Mickelson, *Senior Member, IEEE*

**Abstract**—The electrooptical sampling technique is used to assess the electrical behavior of Ohmic contact regions in GaAs. For this purpose unique Ohmic contact coplanar waveguides were fabricated and tested. A reduced electrooptical sampling signal is detected in certain Ohmic contact regions. Since the electrical fields present in this device are known *a priori*, the deviation of the electrooptical signal from its nominal value is attributed to a deviation in the electrooptical coefficient. Defects introduced during the annealing step of the Ohmic contact accelerated by existing dislocations are discussed as a mechanism capable of disrupting the electrooptic coefficient. A simple phenomenological diffusion model is presented to explain the mechanism responsible for the nulling of the electrooptical coefficient.

## I. INTRODUCTION

THERE have been many techniques employed to observe semiconductor defects. Among these techniques are laser scanning, laser scanning tomography, catholuminescence, photoluminescence, X-ray topography, and many variations of these methods [1]–[6]. The goal of defect recognition is not only to circumvent processing of a seriously defective substrate, but to also determine what seriously defective means. An open question is how do defects influence semiconductor properties and how can their deleterious effects be minimized. To answer these questions, one must know how accurately these defects can be observed, what effects they manifest on the semiconductor properties, and of course, how expensive it will be to minimize certain defects through heat cycling, etc.

Defects will affect device performance. In particular, there have been studies demonstrating the correlation between defects present in the wafer and their influence on device performance. A correlation between microprecipitates and the side gating effect (or crosstalk perturbations) on field effect transistors (FET's) has been studied [7], [8]. This study indicated that small microprecipitates and dislocations can be observed and that their presence directly influences device behavior. Other studies revealed that dislocations in GaAs wafers have been found to influence the threshold voltage of FET's [9] and affect the sheet carrier concentration [10].

Defects are always present in the bulk grown process regardless of process used for growth (LEC, etc.). Recently it has been shown that "memory" of defects exists in epilayers grown on the substrate [11]. That is, regions with

high defect density in the substrate will cause regions grown above these regions to also exhibit high defect densities. An important feature of defect rich crystal regions is that diffusion can occur rapidly through these defect sites [12]. Therefore, if dislocations or other defects are present in the substrate, subsequent processing steps in epitaxial regions above the defect regions could be affected. This will be especially true in the fabrication of an Ohmic contact. The diffusion profile below the electrode occurring during this processing step can be affected by existing dislocations and defects present in the substrate. Metals used in the formation of the Ohmic region can be diffused to much greater than expected depths, therefore, during the annealing process. Indeed, Fillard [12] has shown that there is a rapid variation in the diffusion profile below an Ohmic contact and that a significant defect density of microprecipitates has been found as deep as  $10\ \mu\text{m}$  below the contact with a density of  $10^{16}\text{--}10^{18}\ \text{cm}^{-3}$ .

Electrooptic sampling can be used to noninvasively sample the *in situ* electrical fields of a variety of monolithic microwave integrated circuits (MMIC's) [13]–[17]. The technique uses the local electrooptic coefficient to modulate the test optical pulse. More precisely, a local electric field induces a birefringence in the test electrooptic circuit substrate. The rotation of the plane of polarization is proportional to circuit voltage when the electrooptic coefficient is constant. The technique has been used successfully for testing numerous digital IC's and analog MMIC's [18]–[23].

In this work, we use optical sampling to assess the electrical characteristics of the crystal material located directly below Ohmic contacts. In particular, the electrooptic sampling technique is used to noninvasively determine the electrical behavior of Ohmic contact regions in GaAs. The standard technique [24] for forming an Ohmic contact on a  $n^+$  doped region in GaAs uses a mixture of AuGe–Ni–Au for the electrode formation. The Ohmic process possesses a complicated morphology. This diffusion mechanism may cause unexpected behavior in its crystal properties. For instance, diffusion of a Au–Ge–Ni–mixture behaves differently than the individual diffusion of the metals if they are introduced separately [25]. Further complication arises because the local crystal defects that have grown through the epilayers generate non uniform migration of clusters of atoms during the Ohmic formation step [12].

Since the electrooptic sampling signal is proportional to the integrated electric field between the front and back surfaces of an electrooptic crystal (when a field is applied) weighted by an electrooptic coefficient such as  $r_{41}$  in GaAs, any deviation in

Manuscript received February 22, 1995; revised September 5, 1995. This work was supported by the Army Research Office under Grant DAAL-03-92-G-0289 and by the Office of Naval Research under Grant DOD-ONRN00014-92-J-1190.

The authors are with the Department of Electrical and Computer Engineering, University of Colorado, Boulder, CO 80309-0425 USA.  
IEEE Log Number 9416344.

the electrooptic coefficient from its nominal value will affect the results of the electrooptic sampling measurements. If the defect density introduced into a crystal during contact formation becomes high enough then a disruption in the crystal may be severe enough to affect the electrooptic coefficient. Thus, if the electrooptic coefficient is influenced by a cascade of defects introduced into the substrate then the electrooptic coefficient can be modeled as an activation energy dependent profile based on this diffusion. This will allow a spatially varying electrooptic coefficient to modulate the detected optical signal revealing regions where high density defects exists.

This paper is organized as follows. Section II will discuss the coplanar waveguide (CPW) device tested as well as elucidate some of its electrical properties. This section will also discuss why a CPW test device was chosen. Section III will discuss the electrooptical sampling arrangement as well as address some of the calibration issues and accuracy of the technique. Section IV will then discuss some of the results obtained using the electrooptic sampling apparatus and present a simple phenomenological model based on a diffusion mechanism to explain the measured results. Finally, the conclusion section will review these results.

## II. OHMIC COPLANAR WAVEGUIDE TEST DEVICE

The device tested is shown in Fig. 1 and is a coplanar waveguide (CPW) device with an Ohmic contact introduced by metalization placed over a heavily doped  $n^+$  region in the substrate. The decision to use a CPW test device was based upon the CPW's well known electric field properties. The CPW test device was ideally suited for our electrooptic sampling measurement as well as provided us with other accurate testing measurements (such as network analyzer) to verify that the electric field and transmission characteristics were known a priori. It should be mentioned, however, that the lossy transmission lines were fabricated out of the remaining poor conductor material (the  $n^+$  strip) to study the phase characteristics of lossy lines and to also verify the phase resolution of the electrooptic sampling technique. This work is not presented in this paper.

Initially, the device consisted of a LEC grown wafer with two  $n^+$  epilayers grown on top. The first layer is a 2800 Å epi-layer with a doping density of  $2.1 \cdot 10^{17} \text{ cm}^{-3}$  and the second a 940-Å  $n^{++}$  top epi-layer with a doping density of  $3.9 \cdot 10^{18} \text{ cm}^{-3}$ . Silicon (Si) was used as the dopant. Photoresist was applied in conjunction with a mask to pattern a region to be etched. Wet etching was used to remove the  $n^+$  layers using a  $\text{H}_2\text{SO}_4(98\%)/\text{H}_2\text{O}_2(30\%)/\text{H}_2\text{O}$  solution in the ratio of 1 : 8 : 1000, to leave only 100- $\mu\text{m}$ -wide strips of  $n^+$  layers. The length of these strips varied from 300 to 2000  $\mu\text{m}$ . A new mask was then used to deposit the AuGe(88%Au, 12%Ge)-Ni-Au layer which was then brought to 420° for 90 s completing the Ohmic CPW. This is obviously a very large Ohmic but is ideally suited for studying the effects of diffusion and how this diffusion affects the electrooptic coefficient. The final test device also consists of calibration test strips to calibrate on wafer s-parameter measurements. It

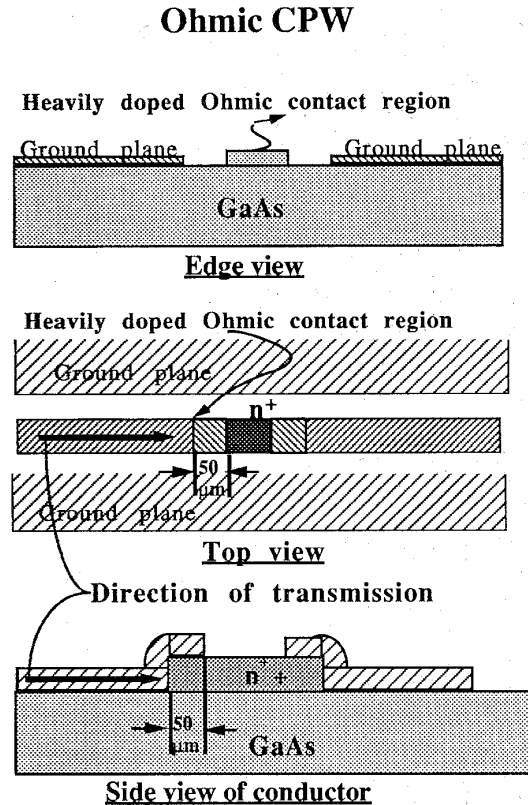


Fig. 1. Ohmic CPW test device.

will now be verified that the test device functions as a lossy transmission line.

Generally, a transmission line can be represented by a lumped element equivalent circuit as shown in Fig. 2. The parameters defining this line are its resistance ( $R(\omega)$ ), inductance ( $L(\omega)$ ), capacitance ( $C(\omega)$ ), and conductance ( $G(\omega)$ ) per unit length. The parameters  $R(\omega)$ ,  $L(\omega)$ ,  $G(\omega)$ , and  $C(\omega)$  are in general frequency dependent. With this model for an equivalent circuit in mind two important characteristics of a transmission line are its characteristic impedance  $Z_o$  and its propagation constant. These can be expressed as follows:

$$Z_o = \sqrt{\frac{R(\omega) + j\omega L(\omega)}{G(\omega) + j\omega C(\omega)}} \quad (1)$$

$$\gamma = \sqrt{(R(\omega) + j\omega L(\omega))(G(\omega) + j\omega C(\omega))}. \quad (2)$$

In these quasi-TEM lines  $R(\omega)$  and  $G(\omega)$  usually represent loss where  $R(\omega)$  is due to the finite conductivity of the metal and  $G(\omega)$  is due to dielectric loss. The inductance ( $L(\omega)$ ) and the capacitance ( $C(\omega)$ ) are obviously the stored magnetic and electrical energy of the circuit and are not generally especially dependent upon frequency but are dependent upon the line geometry [26].

An HP8510 network analyzer was used in conjunction with a calibration program DEEMBED developed by Marks and William at NIST (to do on wafer calibration) to measure the electrical properties of the device [27]–[29]. These measured

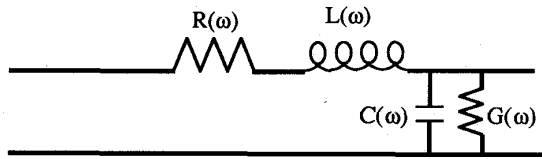


Fig. 2. Transmission line equivalent circuit.

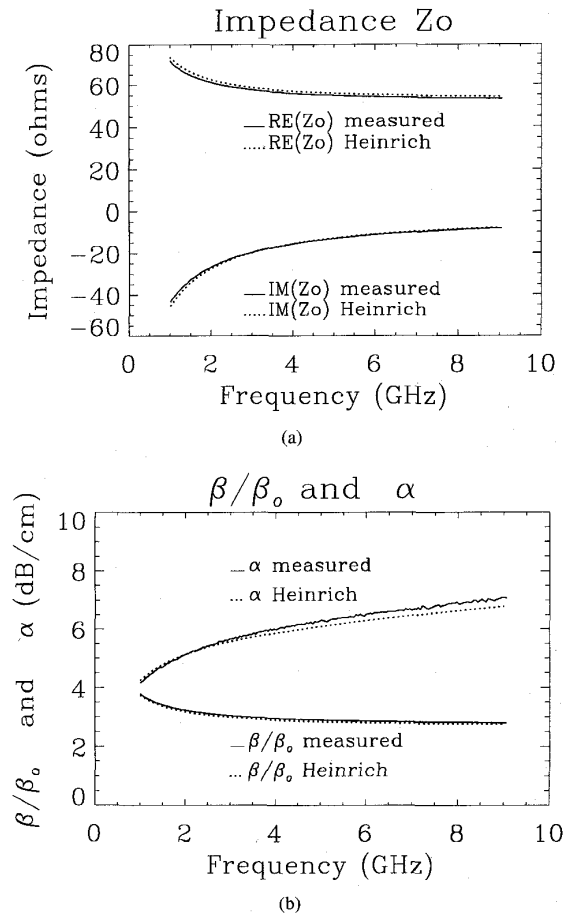


Fig. 3. Transmission Line parameters of calibration strips. (a) Impedance of CPW line—measured versus Heinrich. (b) Propagation constants of CPW line—measured versus Heinrich.

results are compared with computer program developed by Heinrich [26], [30], which takes into account metalization conductivity, thickness, and the dielectric substrate loss for CPW's. In other words the program takes into account the frequency dependence of  $R$ ,  $G$ , and  $L$ ;  $C$  is dependent only upon the geometry. The non-Ohmic test strips are very lossy due to the thin metalization (only about  $1000 \text{ \AA}$  since liftoff was used to remove metalization on the devices). Fig. 3(a) and (b) show the comparison of this program with the measured calibration strips for the propagation constants and impedance of lines which used the same metalization as that found over the  $n^+$  strips. The conductivity used in the calculation was  $1.5 \cdot 10^7$  rather than the bulk value of  $4 \cdot 10^7$ . It is expected

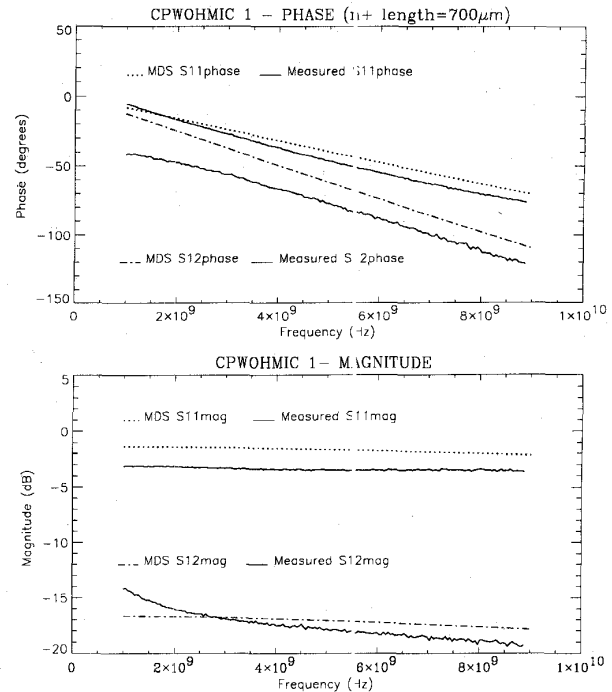


Fig. 4. S-parameters of Ohmic CPW.

that the conductivity would be lower for the evaporated metal. Excellent agreement is observed. S-parameter measurements confirm that the devices behave as very lossy lines. This was expected from the initial design of the CPW's since the  $n^+$  regions have significantly lower conductivity than the metal lines ( $\sigma \approx q\mu_n n$  where  $\sigma$  is the conductivity,  $q$  is the electronic charge,  $n$  is the doping density and,  $\mu_n$  is the mobility assuming all the dopant is ionized and neglecting the hole contribution.  $\sigma = 1/(R_s t)$  can also give the conductivity where  $R_s$  is the measured sheet resistance and  $t$  is the thickness of the doped layer). Fig. 4 shows some typical s-parameter measurements of an Ohmic transmission line compared to the design done by Hewlett Packard's microwave design software (MDS). This particular CPW had a  $700 \mu\text{m}$   $n^+$  strip. The slight discrepancy is due to the frequency dependence of the transmission line parameters (mostly  $R(\omega)$ ).

Transmission line theory was used to confirm that the fields of the CPW are actually known *a priori*. In a CPW, it is known that if a TEM wave is launched along the center conductor of this device, then at any point transverse to the direction of travel along the conductor, the field is constant along this transverse direction (as long as the sampled point is not close to the edge [13]). Therefore we are presented with a slightly different problem in here than the usual problem of determining an unknown field distribution. Here, the fields are known. The detected signal, however, is seen to vary with transverse dimension under some of the contacts which were sampled. Thus we are presented with the task of explaining this behavior. The importance of surface roughness and etalon effects important to the calibration of the electrooptic sampling technique will be addressed in the next section.

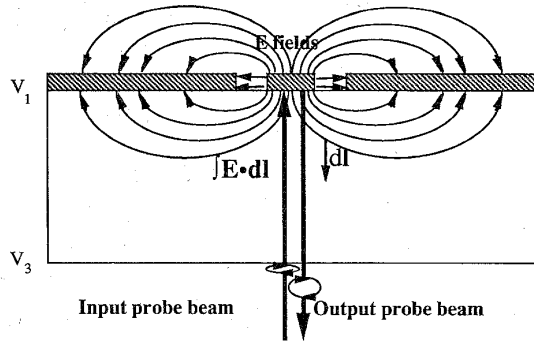


Fig. 5. Optical sampling substrate geometry.

### III. ELECTROOPTIC SAMPLING

The principle of operation of the electrooptic sampling is to use a non-zero electrooptic coefficient of a noncentrosymmetric substrate (GaAs in our case) to polarization modulate a probe beam and then to analyze that probe beam such that the detected signal is proportional to the circuit voltage [13]–[16]. The detected signal is then determined by the integrated electric field along a path normal to the surface as shown in Fig. 5. If the electrooptic coefficient is not uniform throughout the crystal, then the detected voltage can be expressed as

$$I \det \approx V \approx \int r_{41}(x, y, z) E_y(x, y, z) \cdot dl \quad (3)$$

where  $E_y$  is the normal directed field,  $dl$  is the normal path, and  $r_{41}$  is the electrooptic coefficient, which is now a function of position.

Although the lines are quite lossy due to the finite conductivity of the metals, the fields underneath the electrode at any transverse location of the CPW can still be approximated by using the conformal mapping found in Smythe [31] and introduced by Wen [32] for finding the fields of CPW device. The mapping of the CPW into the interior of a rectangle is shown in Fig. 6 and the solutions are shown below

$$E_x = -\frac{v}{K'(k)} \operatorname{Im} \left( \frac{dw}{dz} \right) \quad (4)$$

$$E_y = -\frac{v}{K'(k)} \operatorname{Re} \left( \frac{dw}{dz} \right) \quad (5)$$

$$\frac{dw}{dz} = \frac{1}{K'(k)} \frac{1}{\sqrt{(1-z^2)(1-z^2k^2)}} \quad (6)$$

The solution of the mapping is given by the Jacobi elliptical integral  $z = Sn(w, k)$  where  $k$  is the modulus.  $K(k)$  is the complete elliptical integral of the first kind. Now with this solution it would be merely an academic exercise to integrate the electric field along the normal path  $dl$  if it were not for the addition of the now spatially varying electrooptic coefficient which needs to go inside the integral.

The electrooptic sampling arrangement is shown in Fig. 7. The detection of the optical signal uses time domain techniques analogous to a sampling oscilloscope to heterodyne the electromagnetic signal and the laser pulse. In this case a mode-locked laser pulse with a repetition rate of 76 MHz and pulse

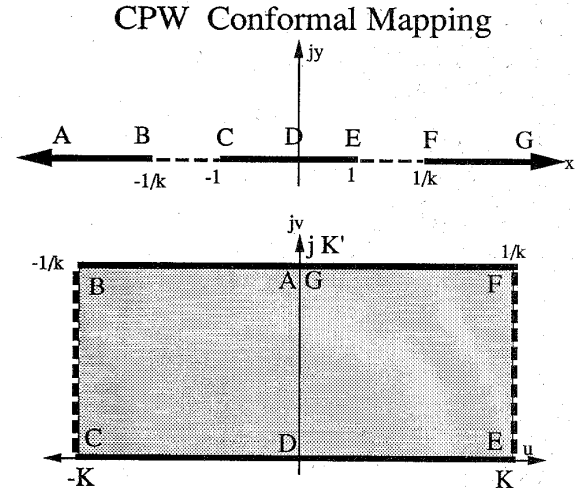


Fig. 6. CPW conformal mapping to determine electric fields.

### Phase and Amplitude Measurement

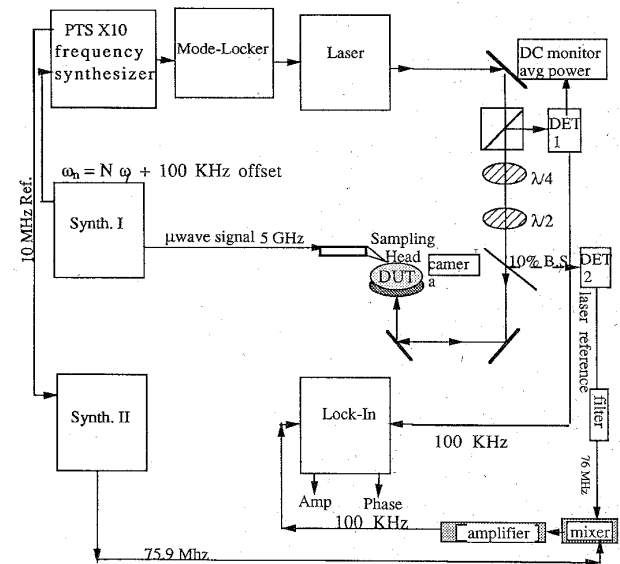


Fig. 7. Optical sampling experimental arrangement.

width of  $\approx 100$  ps is used as the probe beam. It interacts in the substrate with a high frequency electrical field having a frequency a multiple of the laser repetition rate plus an offset (of a 100 kHz) to produce an ac signal of 100 kHz which is an exact multiple of the high frequency electrical signal. The phase of the electrical signal can be recovered by either using a second synthesizer locked to the electrical signal which can be mixed down to the frequency of the detected optical signal to serve as a reference signal fed into lock-in amplifier; or, by deriving the reference wave from the laser pulse itself as shown in the set-up. It is important to note that this system must maintain synchronism between the electrical signal and the laser sampling pulse. The wave plates serve to properly

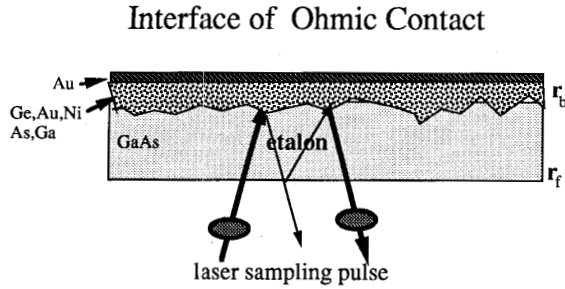


Fig. 8. Etalon geometry.

bias the probe beam so that maximum linear sensitivity is achieved. It should also be noted that the electrooptic sampling system provides two dimensional scans of the test device with position resolution of  $1 \mu\text{m}$ . The spot size of the optical sampling probe beam is  $10 \mu\text{m}$ .

Although electrooptic sampling provides great sensitivity ( $\mu\text{V}/\sqrt{\text{Hz}}$ ), dynamic range (22 dB in GaAs), and is well suited to measuring the modulation of the test optical probe beam due to the local electrooptic coefficient, the detected signal requires careful processing. To accomplish this task, we have developed a calibration procedure for de-embedding the measured data which takes into account weak scattering and etalon effects of the substrate [13]. The success of this calibration procedure has been well documented for the fields of microstrip lines [13]. These calibration issues will be addressed. In particular the following issues will be addressed: 1) the thickness variations in the substrate, 2) the possibility of a spatially varying reflection coefficient, 3) the significance of a high backside reflection coefficient, and 4) scattering effects due to surface roughness.

Our analysis is based on long optical pulses compared to the substrate transit time since our wafer is approximately  $600 \mu\text{m}$  thick and the sampling pulses are approximately 100 ps long. As previously stated [13] the optical probe beam enters an etalon formed by the CPW circuit giving a total reflection coefficient of

$$r(\phi_o) = \frac{-r_f + r_b e^{-i\phi_o}}{1 - r_f r_b e^{-i\phi_o}} \quad (7)$$

where  $r_f$  and  $r_b$  are the effective reflection coefficients of the front and back surfaces of the GaAs substrate, and  $\phi_o$  is the round trip phase delay of the etalon. Fig. 8 shows the etalon geometry set up by the probe beam and the CPW test device. It should be noted, however, that the etalon formed has the laser beam at normal incidence. Writing  $r(\phi_o)$  as

$$r(\phi_o) = |r(\phi_o)| e^{-i\Phi(\phi_o)} \quad (8)$$

and using the notation as stated earlier [13], the signal in the receiver head can be generally expressed as

$$\langle I_o \rangle = |r(\phi_o)|^2 \left[ I_{dc}^o + \frac{\partial \Phi(\phi_o)}{\partial \phi_o} I_{if}^o \right] \quad (9)$$

$I_{dc}^o$  and  $I_{if}^o$  represent the dc and IF receiver signal in the ideal case ( $r(\phi_o) = 1$ ,  $\partial \Phi(\phi_o) = 1$ ) and do not depend on the substrate parameters, but only on the applied electrical

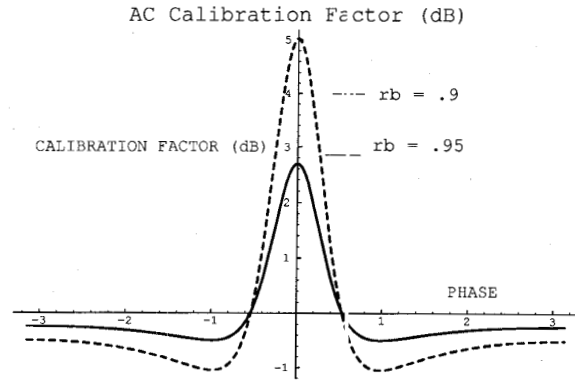
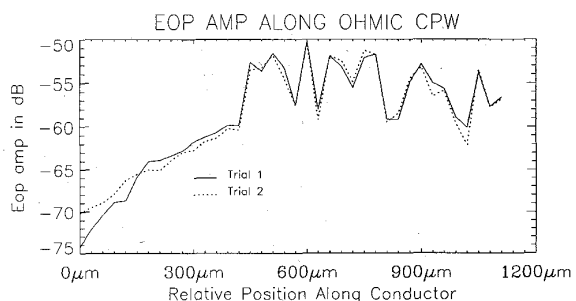


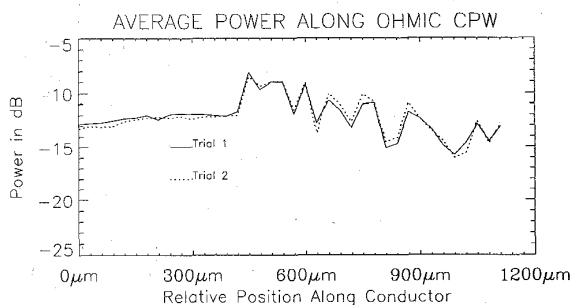
Fig. 9. AC calibration factors present due to the circuit substrate.

field and the wave plate and crystal axes orientation in the sampling head. The term  $\partial \Phi(\phi_o)/\partial \phi_o$  is defined as the partial derivative of the phase function  $\Phi(\phi_o)$  with respect to  $\phi_o$ , where  $\phi_o$  is the phase delay introduced in the etalon. The detected signal is affected by an overall factor of  $|r(\phi_o)|^2$  and the partial derivative factor  $\partial \Phi(\phi_o)/\partial \phi_o$ . The factor  $|r(\phi_o)|^2$  is the dc receiver signal which is measured during the sampling scans and depends on the average total effective reflectivity of the substrate. The partial derivative factor is the wanted polarization rotation modulation giving rise to the ac signal but is also dependent upon the substrate parameters. The above factors will generally be spatially dependent. We have ignored a small scattering parameter which can reduce the effective contrast of the etalon and this will be justified shortly.

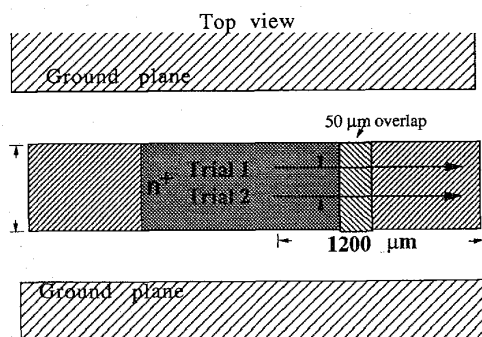
Since the metalization affects the optical properties of the substrate, knowledge of the CPW's fabrication will enable us to approximate the backside reflection coefficient. The front side reflection coefficient is approximated as a smooth optical interface between air and GaAs and is given by  $(n_{\text{GaAs}} - 1)/(n_{\text{GaAs}} + 1) \approx 0.565$  since  $n_{\text{GaAs}} \approx 3.6$ . The metalization of the backside consist of a  $520 \text{ \AA}$  layer of Au-Ge followed by a  $100 \text{ \AA}$  layer of Ni and finally a  $1000 \text{ \AA}$  layer of Au. The index of refraction of these metals are complex and are given as  $(n = n_r + i \cdot n_i$  where  $i = \sqrt{-1}$ )  $n_{\text{Au}} = 0.272 + i7.07$ ,  $n_{\text{Ge}} = 4.42 + i(0.123)$ , and  $n_{\text{Ni}} = 2.85 + i5.10$  (for  $\lambda = 1.06 \mu\text{m}$ ) [33]. The Ge layer does not seem to affect the result to any significant degree. Using a multilayer dielectric stack with complex indices of refraction [34], the back side reflection coefficient of the GaAs metal boundary was determined to be  $|r_b| \approx 0.95$ . The phase is just absorbed into the overall reflection coefficient. The importance of this high backside reflection coefficient is shown in Fig. 9 for  $r_b = 0.95$  and  $r_b = 0.9$ . It is clear from etalon theory that a higher backside reflectivity generally predicts a lower magnitude of correction necessary for the detected reflected electrooptic signal magnitude. Furthermore, since the AC (or electrooptic signal) calibration factor  $\partial \Phi(\phi_o)/\partial \phi_o$  shown as a function of phase retardation in Fig. 9 does not have a very dramatic effect (because of this high reflection coefficient) the dc measured power may prove sufficient to calibrate the data. This dc average power correction is possible because the etalon effects on the average detected power also show



(a)



(b)



(c)

Fig. 10. Measured electrooptical data of Ohmic CPW line. (a) Raw electrooptical sampling detected voltage. (b) Average optical detected Power—used for calibration. (c) Scanning area under CPW line.

up in the same manner in the detected electrooptical signal. Thus, the influence of the etalon is manifest by resulting in a lesser power in the average signal and this in turn also reduces the electrooptical signal by a roughly proportional amount. It should also be noticed that away from the resonance peak (away from where the relative phase is zero) the ac calibration is not significant. Additionally, if the scan was done on a relatively flat region (which DEKTAK measurements indicate in this case) then there would generally not be much calibration involved except for an absolute value factor. Although one would expect scattering from the Ohmic surface, it is primarily Rayleigh scattering and such high angle scattering is not detected by the detector anyway. To justify our calibration we refer to Fig. 10. The sample is scanned twice along the center conductor with the sampling points placed in increments of 30  $\mu\text{m}$  apart. Fig. 10(c) shows the scanning region. Fig. 10(a)

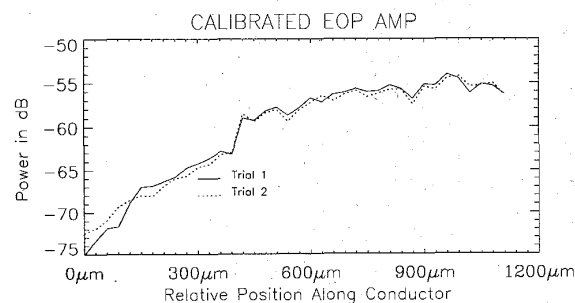


Fig. 11. Calibrated electrooptical sampling data.

shows the electrooptic signal and Fig. 10(b) shows the average optical detected power. It should be noted that the roughness in surface is present in the non Ohmic overlapping metal regions also. The pure  $n^+$  regions are obviously smooth. Trial 2 is the same as scan 1 except that the probe beam is moved 10 mm transversely to the scan in trial 1. The two scans should be identical. Normalizing the detected electrooptic signal to the average optical power appears to calibrate the data quite effectively. This is shown in Fig. 11. This fact is further evidenced in noting that the raw data variations precisely mimic the average power variations. Also, if the average power is constant (indicating very little substrate thickness variation) then the ac calibration factor should not be affected much either since this calibration factor is highly dependent upon these thickness variations. Finally, there could exist a spatially varying reflection coefficient that would complicate the data even more since there are not enough known factors to calibrate this effect. However, this effect would also show up in the dc power scan and therefore it is still possible to provide an accurate calibration. Fig. 10 also demonstrates the repeatability of the data. After completing the initial scans of the test device, the computer control reset the position of the scanning and the entire experiment was repeated to verify the data was not anomalous. This experimental procedure was used on every device tested and no significant anomalous behavior due to experimental error was ever found.

Electrooptic sampling results are sensitive to the electrooptic coefficient. Therefore, lattice disruption (disordering) severe enough to affect the electrooptic coefficient will be observed. Since diffusion has been seen to occur under Ohmic contacts [12], a diffusion model seems appropriate to explain how lattice disruption can take place. Accurate diffusion modeling is complicated. Implanting Si as a dopant (Si was used as our dopant) already has caused impurity induced disordering (IID) [35]. The model to be discussed here will therefore be somewhat qualitative in nature. This simple model describes how diffusion may affect the electrooptic coefficient.

In volumes where a significant amount of microprecipitate diffusion has taken place, it is safe to assume the lattice is disrupted. It might prove useful to compare the integrated electric field (between the front and back surfaces of the circuit substrate) weighted by a constant electrooptic coefficient to that of the integrated electric field (voltage) when the electrooptic coefficient is totally disrupted some known distance

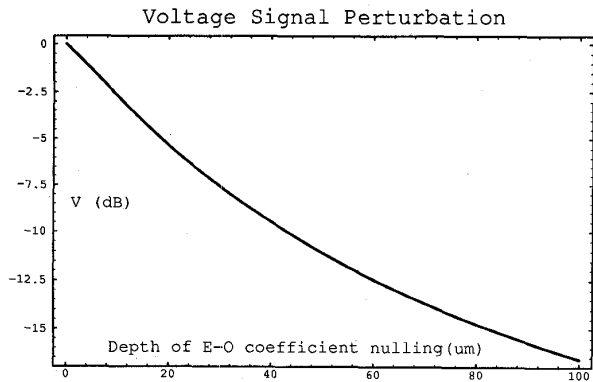


Fig. 12. Deviation in electrooptic signal versus depth of nulled electrooptical coefficient.

below the contact to estimate the order of the effect which would be measured. This is shown in Fig. 12. Although this is a simple model it should be sufficient for at least order of magnitude type calculations. The electric fields used are for a CPW device and the probing beam size is assumed to be a delta function like beam spatially. In this figure the amount of deviation from the ideal voltage signal (in dB) is plotted as a function of the depth from the electrode surface which has had its electrooptic coefficient totally nulled. For example, if in the first 10 m below the device has a zero electrooptic coefficient, then the detected voltage signal would be down  $-3$  dB from its ideal non affected electrooptic coefficient. With a disrupted electrooptic coefficient extending  $20 \mu\text{m}$  into the substrate below the contact electrodes would result in a  $-5.5$  dB reduction in the detected signal. We can compare this resulting variation in signal with that of the measured data shown in Fig. 13. Fig. 13(a) and (b) shows the raw data of an electrooptic scan of a CPW test device. Fig. 13(c) shows the area scanned. It can be seen in this case that the average power along the  $n^+$  and Ohmic regions are very constant. This is generally true for very small scan regions. Therefore no real calibration is necessary here (except for an absolute value correction). Since the high backside reflection coefficient is still present and the average power is relatively constant, the anomalous behavior is due to the variation in the electrooptic signal. This variation, furthermore, is likely due to the Ohmic contact's influence on the electrooptic signal. Here the scanning sampling points are  $10 \mu\text{m}$  apart longitudinally. A maximum variation of  $\approx 8$  dB is observed along the transverse location of the transmission line when present in the Ohmic region. Trials 1, 2, and 3 are all along the center conductor except spaced  $5 \text{ mm}$  apart in the transverse direction. Since the signal should remain constant at any identical transverse location on the CPW this perturbation is due to the electrooptic coefficient and not the applied electric field. This  $8$  dB variation would correspond to the nulling of the electrooptic coefficient down to a depth of approximately  $30 \mu\text{m}$ . This seems higher than one might expect but it is the extreme case measured (of 20 devices fabricated) and gross dislocations in the substrate could account for this behavior. Consideration of our diffusion model will now be addressed.

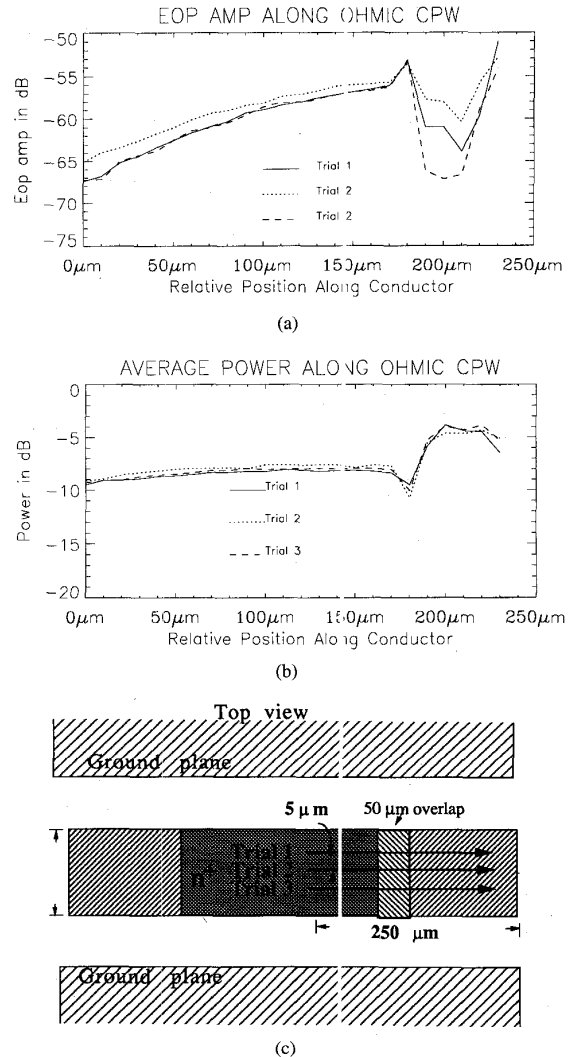


Fig. 13. Measured electrooptical data in the Ohmic region of a CPW line. (a) Raw E-O sampling data. (b) Average optical detected power. (c) Scanning area under CPW line.

The electrooptic signal is given as in (3). Ignoring the spatial extent of the probing beam (the overlap integral of the  $10 \mu\text{m}$  beam will result in a slightly smaller detected perturbation in the signal but to avoid unnecessary complicated expressions will be ignored) the detected signal can again be written as

$$I_{\text{det}} \approx V \approx \int r_{41}(x, y, z) E_y(x, y, z) \cdot dl. \quad (10)$$

It was just demonstrated that a direct nulling of the electrooptic coefficient below the CPW electrode can alter the sampling signal significantly if this destruction occurs over several microns. If the electrooptic coefficient ( $r_{41}$ ) is modified by a diffusion process then this diffusion could explain why our detected signal deviates from the expected. A simple one-dimensional model based on Fick's law of diffusion will be used [36]. Combining Fick's first and second laws gives the following equation and is used for the rate of concentration

impurities diffusing into the GaAs substrate ( $y$  direction):

$$\partial N/\partial t = \partial/\partial y[D\partial N/\partial y] \quad (11)$$

where in general the diffusion coefficient is dependent upon depth if it involves high impurity concentrations [36]. Here,  $N = N(y, t)$  is the concentration of impurities and  $D$  is the diffusion coefficient. However it was observed in Baeumler's work [4] that defects can propagate through the epilayers to the surface. Using this assumption makes the diffusion coefficient constant as a function of depth, but will give the diffusion coefficient a spatial variation (depending where there are defects dictates its magnitude). Therefore, (11) becomes

$$\partial N/\partial t = D(x, z)\partial^2 N/\partial^2 y \quad (12)$$

where  $D(x, z)$  possess spatial variation. If we solve this equation assuming a constant diffusion source the following solution is obtained:

$$N(y, t) = N_o \text{Erfc}[y/(2\sqrt{Dt})]. \quad (13)$$

Here,  $N_o$  is the impurity and  $\text{Erfc}$  is the complementary error function. Since our model is purely phenomenological, the meaning of  $N_o$ ,  $N(y, t)$ , and the diffusion coefficient should be discussed. The diffusion coefficient will assume to follow an Arrhenius behavior and is given by

$$D = D_o \exp[-E_A/(kT)] \quad (14)$$

where  $D_o$  is the diffusion constant,  $k$  is the Boltzman constant,  $T$  is the temperature at which the diffusion takes place, and  $E_A$  is the activation energy. High temperatures normally involved in diffusion models mitigate the sensitivity of the activation energy. However, in our model the activation energy is viewed as simply a defect activated energy dependent upon the defect concentration and is highly sensitive to small variations in the defect concentration. Additionally, since the diffusion constant is unknown these values need to be determined. Fig. 14 shows the variation of the diffusion  $N(y, t)/N_o$  as a function of depth in  $\mu\text{m}$  for various diffusion constants and activation energies. There is dramatic effect on  $N(y, t)/N_o$  for different activation energies. The activation analogy corresponds to the ability of the presence of defects to rapidly increase diffusion below the electrode. However, the effect  $N(y, t)/N_o$  has on the disruption of the electrooptic coefficient needs clarification. If we assume that as long as  $N(y, t)/N_o$  exceeds some nominal value of 1% results in a volume with a greatly reduced electrooptic coefficient, then Fig. 15 shows that an activation energy of 1.3eV and diffusion constant of  $10 \text{ cm}^2/\text{s}$  dictates that this volume extends to a depth of approximately  $20 \mu\text{m}$ . Using this hard limit of

$$r_{41} = \begin{cases} r_{41}, & N(y, t)/N_o < .01 \\ 0, & N(y, t)/N_o > .01 \end{cases} \quad (15)$$

results in agreement with our measured data. The assumption of the 1% rule generally refers to interstitial defects. The meaning of  $N(y, t)/N_o$  could be that if the precipitate defects are, for example,  $100 \text{ nm}^3$  then they would need a density of  $10^{17} \text{ cm}^{-3}$  in order that  $N(y, t)/N_o = 0.01$ . These numbers comparably agree with [12].

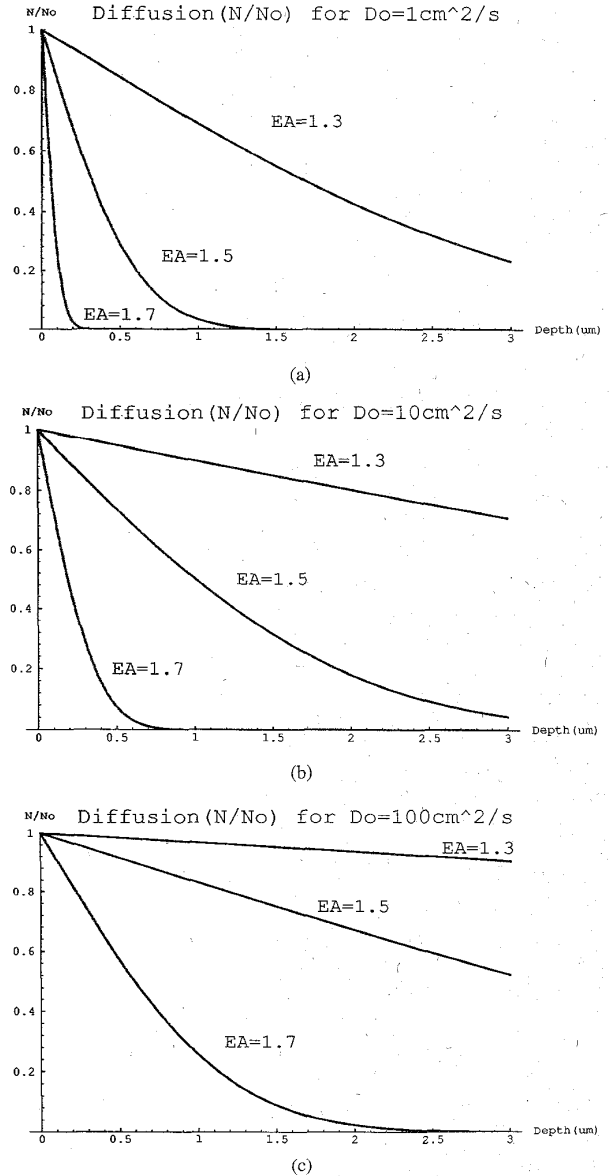


Fig. 14. Effective defect concentration Vs depth below Ohmic surface. (a) Diffusion constant =  $1 \text{ cm}^2/\text{s}$ ,  $E_A = 1.3, 1.5, 1.7 \text{ eV}$ . (b) Diffusion constant =  $10 \text{ cm}^2/\text{s}$ ,  $E_A = 1.3, 1.5, 1.7 \text{ eV}$ . (c) Diffusion constant =  $100 \text{ cm}^2/\text{s}$ ,  $E_A = 1.3, 1.5, 1.7 \text{ eV}$ .

#### IV. CONCLUSION

We have presented the results of electrooptical sampling on unique Ohmic contact coplanar waveguides (CPW's). A reduced electrooptical sampling signal was detected in certain Ohmic contact regions. This reduced signal is attributed to a nulling of the electrooptical coefficient. A mechanism contributing to the reduced electrooptical coefficient is presented and is based on a phenomenological model incorporating diffusion processes. This model takes into account defects introduced into the substrate during the annealing step of Ohmic contact fabrication that may be severe enough to disrupt the crystal properties that would result in a reduced

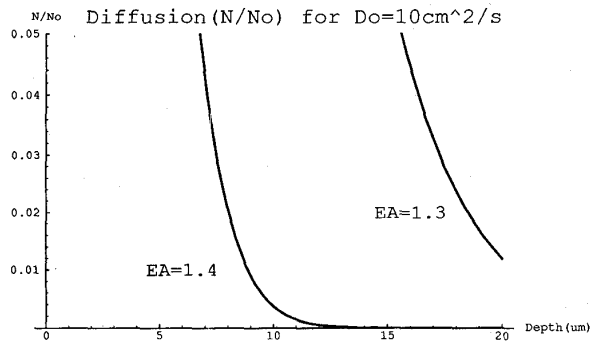


Fig. 15. Effective defect concentration for  $D_o = 10 \text{ cm}^2/\text{s}$ ,  $E_A = 1.3$  and  $1.4 \text{ eV}$ .

electrooptical coefficient. This simple diffusion model uses a spatially varying activation energy based on the defect density and agrees with our results. It appears that electrooptical sampling can detect a reduction of the electrooptic coefficient due to this diffusion process. Calibration issues concerning the electrooptical sampling technique are addressed and do not appear to effect the measured data significantly.

It should be noted that we have used electrooptical sampling in a different manner than the usual procedure of determining unknown field distributions. Here, the fields are known but the electrooptic coefficient is seen to vary spatially below the Ohmic surface. This new application of electrooptical sampling could be used, for example, to possibly measure the electrooptic coefficient perturbation present in  $\text{LiNbO}_3$  waveguides when proton exchange ( $\text{H}^+$  ions) occurs or Ti in diffusion takes place. Furthermore, a low frequency version of optical sampling technique could be used for more expedient and less sophisticated instrumentation to measure semiconductor characteristics.

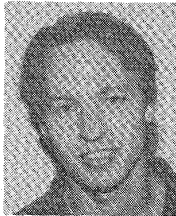
#### ACKNOWLEDGMENT

The authors are grateful for the valuable discussions with J. P. Fillard, M. Castagné, P. C. Montgomery of the Laboratoire LINC-S-CEM Université de Montpellier, and with M. Baeumler and W. Jantz of the Fraunhofer Institut für Angewandte Festkörperphysik.

#### REFERENCES

- [1] C. Miner, "Pre-processing epitaxial layer evaluation: What do you really measure?," *Inst. Phys. Conf. Ser.* no. 135, ch. 5, pp. 147–156, 1994.
- [2] V. P. Kalinushkin, N. V. Safronov, and N. A. Sulimov, "Spatial orientation study of microprecipitates in Semi-insulating GaAs crystals by IR light scattering technique," *Inst. Phys. Conf. Ser.* no. 135, ch. 4, pp. 143–146, 1994.
- [3] P. Franzosi and H. Bernardi, "Investigation of extended crystal defects in HgCdTe epilayers on CdTe, CdZnTe and CdTe/sapphire," *Inst. Phys. Conf. Ser.* no. 135, ch. 9, pp. 319–322, 1994.
- [4] M. Baeumler, E. C. Larkins, K. H. Bachem, D. Bernkhan, H. Riechert, J. D. Ralston, and W. Jantz, "Influence of substrate dislocations on epitaxial layers studied by photoluminescence microscopy and topography," *Inst. Phys. Conf. Ser.* no. 135, ch. 5, pp. 169–172, 1994.
- [5] P. Gall, J. P. Fillard, M. Castagné, J. L. Weyher, and J. Bonnafé, "Microtomography observation of precipitates in semi-insulating GaAs materials," *J. Appl. Phys.*, vol. 64, no. 10, p. 15, Nov., 1988.
- [6] J. P. Fillard, P. C. Montgomery, P. Gall, M. Castagné, and J. Bonnafé, "High resolution and sensitivity infrared tomography," *J. Crystal Growth*, vol. 103, pp. 109–115, 1990.
- [7] J. P. Fillard, M. Castagné, P. Gall, and J. Bonnafé, "Transistor specifications and substrate defects in GaAs test circuits," *J. GaAs Applied Symp.*, Rome, 1990.
- [8] M. Castagné, J. P. Fillard, D. Achvar, F. Gall, "LST-detected microprecipitates and their role in the performance of GaAs integrated circuits," *Semiconduct. Sci. Technol.*, vol. 7, pp. A146–A149, 1992.
- [9] S. Miyazawa, Y. Ishii, S. Ishida, Y. Nanishi, "Direct observation of dislocation effects on threshold voltage of a GaAs field-effect transistor," *Appl. Phys. Lett.* vol. 43, no. 9, p. 1, Nov. 1983.
- [10] F. Hyuga, "Effect of dislocations on sheet carrier concentration of Si-implanted, semi-insulating, liquid-encapsulated Czochralski grown GaAs,"
- [11] Z. M. Wang, M. Baeumler, W. Jantz, K. H. Bachem, E. C. Larkins, and J. D. Ralston, "Photoluminescence microscopy investigation of lattice defects in epitaxial heterostructures," *J. Cryst. Growth*, vol. 126, pp. 205–215, 1993.
- [12] J. P. Fillard, M. Castagné, P. C. Montgomery, J. Bonnafé, P. Gall, E. Baudry, and D. Montaner, "Latest results in interface image reconstruction: Application to ohmic contact inspection," *Inst. Phys. Conf. Ser.* no. 135, ch. 4 pp. 109–116, 1994.
- [13] D. R. Hjelme and A. R. Mickelson, "Voltage calibration of the direct electrooptic sampling technique," *IEEE Trans. Microwave Theory Tech.*, vol. 40, no. 10, pp. 1941–1950, 1992.
- [14] J. A. Valdmans and G. Mourou, "Sub-picosecond electro-optic sampling: Principles and applications," *IEEE J. Quantum Electron.*, vol. QE-22, pp. 69–78, 1986.
- [15] B. H. Kolner and D. M. Bloom, "Electrooptic sampling in GaAs integrated circuits," *IEEE J. Quantum Electron.*, vol. QE-22, pp. 79–93, 1986.
- [16] K. J. Weingarten, M. J. Rodwell, and D. M. Bloom, "Picosecond optical sampling of GaAs integrated circuits," *IEEE J. Quantum Electron.*, vol. 24, pp. 189–220, 1988.
- [17] J. M. Wiesenfeld, "Electro-optic sampling of high-speed devices and integrated circuits," *IBM J. Res. Develop.*, vol. 34, pp. 141–161, 1990.
- [18] R. Majidi-Ahy, K. J. Weingarten, M. Riazati, B. A. Auld, D. M. Bloom, "Electrooptic sampling measurements of coplanar waveguide modes," *Electron. Lett.*, 23, pp. 1262–1263, 1988.
- [19] K. J. Weingarten, M. J. Rodwell, and D. M. Bloom, "Picosecond optical characterization of GaAs integrated circuits," *Gallium Arsenide Tech.*, vols. II–III, D. K. Ferry, Ed., 1987.
- [20] J. L. Freeman, S. K. Diamond, H. Fong, and D. M. Bloom, "Electro-optic sampling of planar digital GaAs integrated circuits," *Appl. Phys. Lett.*, vol. 47, pp. 1083–1084, 1985.
- [21] M. J. Rodwell, K. J. Weingarten, J. L. Freeman, and D. M. Bloom, "Gate propagation delay and logic timing of GaAs integrated circuits measured by electro-optic sampling," *Electron. Lett.*, vol. 22, pp. 499–501, 1986.
- [22] X. C. Zhang and R. K. Jain, "Measurement of on-chip waveforms and pulse propagation in digital integrated circuits by electro-optic sampling," *Electron. Lett.*, vol. 22, pp. 264–265, 1986.
- [23] J. M. Wiesenfeld, R. S. Tucker, A. Antreasyan, C. A. Burrus, A. J. Taylor, V. D. Matterna, P. A. Garbinski, "Electro-optic sampling measurements of high speed InP integrated circuits," *Appl. Phys. Lett.*, 50, pp. 1310–1312, 1987.
- [24] N. Braslau, "Ohmic contacts to GaAs," *Thin Solid Films*, vol. 104, pp. 391–397, 1983.
- [25] M. Heiblum, M. I. Nathan, and C. A. Chang, "Characteristics of AuGeNi Ohmic contacts to GaAs," *Solid State Electron.*, vol. 25, no. 3, pp. 185–195, 1982.
- [26] W. Heinrich, "Full-wave analysis of conductor losses on MMIC transmission lines," *IEEE Trans. Microwave Theory Tech.*, vol. 38, no. 10, pp. 1468–1472, 1990.
- [27] R. B. Marks, "A multiline method of network analyzer calibration," *IEEE Trans. Microwave Theory Tech.*, vol. 39, no. 7, pp. 1205–1215, 1991.
- [28] R. B. Marks and D. F. Williams, "Characteristic impedance determination using propagation constant measurement," *Microwave Guided Wave Lett.*, vol. 1, no. 6, pp. 141–143, 1991.
- [29] D. F. Williams and R. B. Marks, "Transmission line capacitance measurement," *Microwave Guided Wave Lett.*, vol. 1, no. 9, pp. 243–245, 1991.
- [30] W. Heinrich, "Quasi-TEM Description of MMIC Coplanar Lines Including Conductor-Loss Effects," *IEEE Trans. Microwave Theory Tech.*, vol. 41, no. 1, pp. 45–52, 1993.
- [31] W. R. Smythe, *Static and Dynamic Electricity*, third ed. New York: Hemisphere, pp. 101–102, 1989.

- [32] C. P. Wen, "Coplanar waveguide: A surface strip transmission line suitable for non reciprocal gyromagnetic device application," *IEEE Trans. Microwave Theory Tech.*, vol. MTT-17, pp. 1087-1090, 1969.
- [33] E. D. Palik, Ed., *Handbook of Optical Constants fo Solids I-II*. New York: Academic.
- [34] M. Born and E. Wolf, *Principles of Optics*, sixth ed. Oxford, U.K.: Pergamon, 1980.
- [35] B. Chen, Q. M. Zhang, and J. Bernhok, "Si diffusion in GaAs and Si-induced interdiffusion in GaAs/AlAs superlattices," *Phys. Rev. B*, vol. 49, no. 4, pp. 2985-2988, 1994.
- [36] R. C. Jaeger, *Introduction to Microelectronic Fabrication*, vol. 5, Modular Series on Solid State Devices, G. W. Neudeck and R. F. Pierret, Eds. Reading, MA: Addison-Wesley, 1989.



**Paul D. Biernacki** was born on January 31, 1966, in New Orleans, LA. He received the B.A. degree in physics from Louisiana Tech University, Ruston, LA, in 1989 and the M.S. degree in electrical engineering in 1993 from the University of Colorado, Boulder, and is currently working toward the Ph.D. degree in electrical engineering at the University of Colorado, Boulder.

From 1990 to 1993, he was a recipient of a four-year DOE Fellowship program and was working on computer generated holography at the Optoelectronic Computing Systems Center NSF/Engineering Research Center. His current research interests include microwave optics, electrooptic sampling, holography, and diffractive optics.

**Henry Lee**, photograph and biography not available at the time of publication.



**Alan R. Mickelson** was born on May 2, 1950, in Norwalk, CT. He received the B.S.E.E. degree from the University of Texas, El Paso, in 1973, and the M.S. and Ph.D. degrees from the California Institute of Technology, Pasadena, in 1974 and 1978, respectively.

He spent a postdoctoral year at Caltech in 1978-1979 before going to the Byurakan Astrophysical Observatory, Byurakan, Armenian S.S.R. (presently Armenia) for 1979-1980.

Following a period in Armenia, he joined the Elektronikkaboratoriet (Electronics Research Laboratory) of the Norwegian Institute of Technology, at first as an NTNF Postdoctoral Fellow, and later as a staff scientist. His research in Norway primarily concerned characterization of optical fibers and fiber compatible components and devices. In 1984, he joined the Department of Electrical and Computer Engineering of the University of Colorado, Boulder, where he became Associate Professor in 1986. His present research concerns integrated optical device fabrication and characterization, microwave measurement and device characterization, as well as application of optical devices and techniques in high speed systems.

In 1980, Dr. Mickelson received an honorable mention from the IEEE Antennas and Propagation Society for the paper of the year award, for a paper taken from his thesis, which was written under the supervision of Prof. C. Papas. He has published more than 60 articles in refereed publications and has graduated 13 Ph.D. students at present, all of whom are still gainfully employed in technical fields.